Vehicular Positioning Using 5G Millimeter Wave and Sensor Fusion in Highway Scenarios

Seyed Samie Mostafavi*, Stefano Sorrentino†, Mehmet Burak Guldogan†, Gabor Fodor*†
*KTH Royal Institute of Technology, †Radio Research, Ericsson
Emails: ssmos@kth.se {stefano.sorrentino, burak.guldogan, gabor.fodor}@ericsson.com

***Abstract*—The performance of Global Navigation Satellite System (GNSS)-based positioning techniques degrades in tunnels, urban canyons and other areas, in which GNSS coverage is poor. Recent advances indicate that radio-based positioning techniques have the potential of complementing GNSS-based positioning services in such problematic areas. In this work, we propose to combine range and angle measurements routinely exercised by fifth generation of mobile communication (5G) base stations with acceleration measurements by vehicles to generate position estimates. Specifically, we propose to utilize an extended Kalman filter to combine the range, angle and acceleration measurements. The accuracy of this positioning system is studied in millimeter-wave 5G cellular networks. Specifically, the proposed positioning system using 5G and sensor fusion is tested in a highway scenario in which 5G base stations provide cellular coverage. In this setting, we study the impact of certain parameters of the 5G network such as the available bandwidth and the propagation environment on the positioning accuracy. We find that the positioning accuracy is largely affected by the number of antennas in the base station and that the proposed scheme outperforms GNSS based schemes in the problematic areas.**

***Index Terms*—5G networks, positioning, sensor fusion, Kalman filter, millimeter wave**

I. Introduction

Due to recent advances in the telecommunications industry, vehicles connected to cellular networks are becoming available and more popular. Through this connection, vehicles will be able to communicate with each other and with the network infrastructure to share important data. Using such data, accidents can be prevented and lives can be saved [1]. Position and the kinematic state of the vehicle are critical pieces of information for safety applications. Indeed, high accuracy positioning enables advanced driver-assistance systems and makes autonomous cars able to execute safety-related maneuvers [2].

In general, a position is calculated by taking into account measurements of distances or angles to some reference points whose positions are known. In a two-dimensional plane, three reference points are enough to compute a position. This positioning problem has been tackled in different schemes for various scenarios and requirements. The most widely used solution for vehicular positioning relies on Global Navigation Satellite Systems (GNSS) such as the Global Positioning System. The average accuracy of GNSS ranges from a few meters to above 20 m, limiting its application in autonomous vehicles as decimeter-level accuracy is needed to stay in lane. In addition, all GNSS based solutions show significant performance loss in dense urban driving environments due to poor satellite coverage [3].

To address the GNSS limitations, there have been important studies on radio-based positioning techniques including those used in 5G systems. Compared to currently deployed cellular networks, 5G is bringing huge improvements in capacity, number of connected devices, and latency. These qualities are made possible by higher bandwidths and advanced antenna systems. In 5G, technologies such as millimeter wave (mmWave) and multiple-input-multiple-output (MIMO) are used, where both the user equipment (UE) and the base station have arrays of large number of antennas, and work at a frequency in the range of 30-300 GHz having access to large bandwidths. Recent research works show that these features make 5G mmWave systems favorable for submeter accuracy positioning [4].

Several works aiming to extract the benefits of the next generation of cellular networks for positioning have been published recently. At mmWave frequencies, large bandwidths are available which enable more accurate time of arrival (TOA) or time difference of arrival measurements. These measurements can be advantageously used for range estimation utilizing that ranging from at least 3 fixed nodes or anchors (in 2-dimensional space) using multilateration can be used to a position estimation [5]. Despite its promising accuracy, multi-anchor positioning is not practical at cellular networks, in which any signal which is received from the base stations other than the serving one on the same frequency is considered as interference [6]. Furthermore, in mmWave frequencies the path loss is typically high and beamforming gain is required to compensate the path loss. On the other hand, due to the high frequency of mmWaves, more antennas can be packed in the same area which enables accurate angle of departure (AOD) and angle of arrival (AOA) estimations. Hence, in mmWave systems, the combination of AOD or AOA with TOA measurements makes position estimation theoretically possible with a single anchor. In reference [7], closed-form error bound expressions for range and angle estimations in line of sight (LOS) scenarios are derived.

In this work, we propose to fuse range and angle measurements routinely exercised by 5G mmWave cellular base stations with acceleration measurements by vehicles to generate position estimates of moving vehicles. Specifically, we propose to utilize an extended Kalman filter to combine these measurements. The proposed positioning approach is tested in a simulated highway scenario in which 5G base stations

provide cellular coverage. We find that utilizing the inertial measurement unit (IMU) can help GNSS in the outage periods and specifically, it can compensate high errors of 5G based positioning systems during LOS outages.

II. System Model

A. Geometry

The network based positioning in this work is based on the downlink MIMO communication between a vehicle mounted UE and some base stations. The UE receives the power from all of the base stations but the energy from the closest base station is desirable and others are considered as the interference. Based on the spherical coordinate system, as shown in Figure 1, a base station transmits a static grid-of-beams from the uniform rectangular array (URA) antenna which is placed on $\mathbf{p}_T = [x_T; y_T; z_T]^T$ with the orientation $\mathbf{o}_T = [\ _{0,T};\ _{0,T}]^T$ and the UE at the time step k, receives the waveform on the URA antenna which is placed on $\mathbf{p}_{R,k} = [x_{R,k}; y_{R,k}; z_{R,k}]^T$ with the orientation $\mathbf{o}_{R,k} = [\ _{0,R,k};\ _{0,R,k}]^T$ [8] [1].

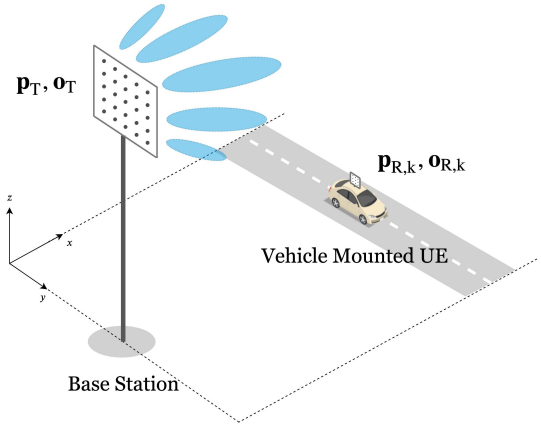

Fig. 1: The MIMO communication system model between a base station with a 5×5 URA antenna and a vehicle with a 3×3 URA antenna.

Since in this work it is assumed that the UE is always on the xy-plane, the rotations outside the xy-plane are not modeled. These rotations happen when the vehicle goes up or down hills and its elevation changes. However, changes in are important when the vehicle turns left or right and the tilt angle of the UE antenna changes.

B. Channel Model

Considering a transceiver system equipped with N_R receive antennas and N_T transmit antennas that supports elevation and azimuth beamforming, assuming that only LOS path is present, the narrow band channel matrix can be expressed in terms of transmit and receive array responses as [9], in the form

$$\mathbf{H} = \mathbf{a}_R B \mathbf{a}_T^T \in C^{N_R \quad N_T}; \tag{1}$$

where $\mathbf{a}_R$ and $\mathbf{a}_T$ are the related receive and transmit unit-norm array response vectors respectively, B is the total path gain and is the complex gain of the LOS path without considering array antenna gains and they are modeled by $B = \sqrt{N_T N_R}$ where

$$= |\ |e^{j2\ D=}\ ;|\ | = \frac{}{(4\ D)^{2:31}}; \tag{2}$$

$D = ||\mathbf{p}_T - \mathbf{p}_R||$ is the distance between the transmitter and the receiver, and $|\ |$ is representing the path loss model. The chosen model for the signal power estimation over the distance is the free space path loss model. The model's path loss exponent is calculated by [10] based on the Monte Carlo simulations of the 3rd generation partnership project (3GPP) rural macro (RMa) LOS path loss model.

Assuming the LOS path, denote AOD by $(\ _T;\ _T)$ and AOA by $(\ _R;\ _R)$ where the related unit-norm array response vectors are given by

$$\mathbf{a}_T(\ _T;\ _T)\ ,\ \frac{1}{\sqrt{N_T}} e^{\ j\boldsymbol{\Delta}_T^T \mathbf{k}(\ _T;\ _T)} \in C^{N_T}; \tag{3}$$

$$\mathbf{a}_R(\ _R;\ _R)\ ,\ \frac{1}{\sqrt{N_R}} e^{\ j\boldsymbol{\Delta}_R^T \mathbf{k}(\ _R;\ _R)} \in C^{N_R}; \tag{4}$$

where $\mathbf{k}(\ _R;\ _R) = \frac{2}{}[\cos\ \sin\ ; \sin\ \sin\ ; \cos\ ]^T$ is the wavenumber vector, is the wavelength, $\boldsymbol{\Delta}_R$, $[\mathbf{u}_{R;1}; \mathbf{u}_{R;2}; :::; \mathbf{u}_{R;N_R}]$; $\mathbf{u}_{R;n}$, $[x_{R;n}; y_{R;n}; z_{R;n}]^T$ is a vector of Cartesian coordinates of the n^{th} receiver element which are derived from $\mathbf{p}_R$ and $\mathbf{o}_R$. $\boldsymbol{\Delta}_T$ and $\mathbf{u}_{T;n}$ are defined similarly.

Considering the narrow-band array model and denoting the TOA of the LOS path by , the channel can be expressed as

$$\mathbf{H}(t) = \sqrt{N_R N_T}\ \ \mathbf{a}_R \mathbf{a}_T^H\ (t - \ ) \in C^{N_R \quad N_T}. \tag{5}$$

C. Transmission Model

It is assumed that the transmitter sends a signal in N_B directional beams in the space with N_s symbols in time as

$$s_l(t) = \sum_{k=0}^{N_s\ 1} a_{l;k} p(t - kT_s); \quad 1 \le l \le N_B; \tag{6}$$

where T_s is the symbol duration, $a_{l;k}$ are known pilot symbols with unit energy, transmitted over the l^{th} beam, and $p(t)$, is a pulse with unit energy. The pilot signal is defined as $\mathbf{s}(t)$, $[s_1(t); s_2(t); :::; s_{N_B}(t)]^T$ with the bandwidth W and in the output of the transmitter it is multiplied by a directional beamforming matrix defined as

$$\mathbf{F}\ ,\ [\mathbf{f}_1(t); \mathbf{f}_2(t); :::; \mathbf{f}_{N_B}(t)] \in C^{N_T \quad N_B}; \tag{7}$$

$$\mathbf{f}_l = \frac{1}{\sqrt{N_B}} \mathbf{a}_{T;l}(\ _l;\ _l); \quad 1 \le l \le N_B. \tag{8}$$

In order to keep the transmitted power fixed with different N_T and N_B, it can be shown that $Tr(\mathbf{F}^H \mathbf{F}) = 1$ and $E[\mathbf{s}(t)\mathbf{s}^H(t)] = \mathbf{I}_{N_B}$. Therefore, the transmitted signal is in the form

$$\mathbf{e}(t) = \sqrt{E_s}\mathbf{F}\mathbf{s}(t) \in C^{N_T}; \tag{9}$$

where E_s is the transmitted energy per symbol duration.

[1] The subscripts T and R refer to the transmit and receive sides, respectively.

D. Received Signal

Assuming there is only one transmitter, the received signal considering above definitions can be expressed as

$$\mathbf{r}(t) = \mathbf{H}(t) \sim \mathbf{e}(t) + \mathbf{n}(t) \in \mathbb{C}^{N_R}; \tag{10}$$

where $\mathbf{n}(t)$, $[n_1(t); n_2(t); :::; n_{N_R}(t)]^T \in \mathbb{C}^{N_R}$ is white Gaussian zero-mean noise with power spectral density of N_0. In order to elaborate Equation 10, the transmission model term and the channel model term are replaced from Equations 9 and 5 respectively and the result is

$$\mathbf{r}(t) = \sqrt{N_R N_T E_s}\ \mathbf{a}_R \mathbf{a}_T^H \mathbf{F} \mathbf{s}(t - \ ) + \mathbf{n}(t) \in \mathbb{C}^{N_R}: \tag{11}$$

Considering the received signal is periodic with T_S and $E_s = P_T T_s$, also assuming that due to the small number of elements the receiver antenna is near isotropic, the received signal power without noise can be expressed as

$$P_R = P_T\ N_T N_R\ ||\mathbf{a}_T \mathbf{F}||^2\ |\ |^2: \tag{12}$$

In this research's experiments, more than one transmitter are present in the network. Hence, when the connected base station (indicated with i) transmits the signal, the UE receives the thermal noise with the power $N_0 W$, other base station's signals (indicated with j) with the total power of $P_{R;j}$, and the transmitted signal which is affected by the beamforming and pathloss. The interference is assumed white and Gaussian and it is added to the noise power, where $N_0 = -170$ dBm/Hz is the power spectral density of the noise.

E. 5G Measurements Model

Having defined the communication model, we provide Cramér-Rao lower bounds (CRLB) derivations for range and angle of departure with respect to the base station. To obtain the CRLB of AOD,AOA, and TOA in the predefined communication model, we define the parameter vector in the form φ , $[\ _R;\ _T;\ _R;\ _T;\ ]^T$. The channel parameters that are important for the downlink positioning are AOD in the form $(\ _T;\ _T)$ and TOA in the form . The closed-form formulas for the CRLBs of these channel parameters are derived to be used in the 5G measurements model according to [7].

For the simplicity, it is assumed that during the simulation, the elevation of the vehicle does not change. Hence, from now on, the 5G measurements are the range r_k and the transmit angle $_k$, $_{T;k}$ with respect to the base station.

In order to simulate a single anchor positioning system, we need to generate angle and range samples. By the means of CRLB closed-form formulas, the standard deviation of the error in angle measurement and ranging for each and every point on the xy-plane can be calculated. As shown in Figure 2, for generating the samples at time step k, an ideal estimator is assumed that adds white Gaussian noise to the true angle and range values of the UE in the form

$$r_k = \ _k + \sqrt{(x_{R,k} - x_T)^2 + (y_{R,k} - y_T)^2}; \tag{13}$$

$$_k = \ _k + arctan\left(\frac{y_{R,k}\ \ y_T}{x_{R,k}\ \ x_T}\right); \tag{14}$$

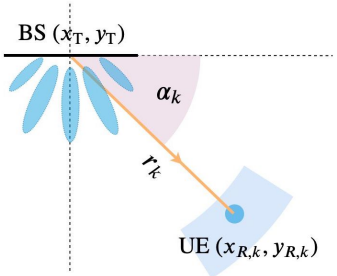

Fig. 2: 5G range r_k and angle $_k$ measurement model.

where $_k \sim \mathcal{N}(0;\ ^2)$ and $_k \sim \mathcal{N}(0;\ ^2)$ are white Gaussian samples with the standard deviations given by

$$= (\sqrt{\text{CRLB}(\ )} \times c): \sin\ _T; \tag{15}$$

$$= \sqrt{\text{CRLB}(\ _T)}; \tag{16}$$

where c is the speed of light, CRLBs are obtained from the closed-form formulas in [7], and calculated using the setup parameters and the position and orientation of the UE. Multiplication of $\sin\ _T$ is necessary because the CRLB is calculated in 3D space and the result should be on 2D xy-plane. The noiseless terms of Equations 13 and 14 are true range and true angle of the UE from the connected base station (BS) respectively.

F. LOS Blockage Model

As mentioned earlier, the performance of positioning techniques in LOS blocked situations drops significantly and in this work, the radio measurements are only available when the LOS is available. This model captures whether the communication between the UE and BS is possible or not. According to 3GPP technical report [11], assuming d_{2D} is the distance from UE to BS in xy-plane, for the RMa environment the corresponding LOS probability function is derived in the form

$$\text{Pr}_{\text{LOS}}^{\text{RMa}} = \begin{cases} 1 & d_{2D} \leq 10m \\ \exp\left(-\frac{d_{2D}\ \ 10}{1000}\right) & d_{2D} > 10m: \end{cases} \tag{17}$$

This equation does not provide information about the duration or arrival rate of the blockage events.

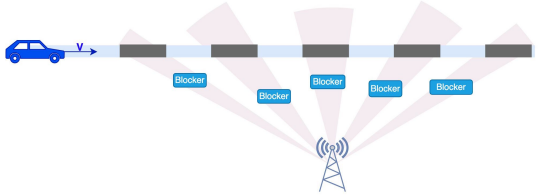

Fig. 3: Blockage scenario with 50% LOS blockage probability.

Two independent models in the space domain (xy-plane) are used for LOS blockage arrival rate and LOS blockage duration. Usually the blockage models are in the time domain but in this paper we assume the models are static and restricted to be in the xy-plane. For mathematical simplicity, we assume the

blockage duration is exponentially distributed with parameter $_B$ which represents the expected length of a blockage event in meters.

For LOS blockage arrival rate the model is a Poisson distribution with parameter $_B$ which is the expected number of blockage occurrences per unit distance (meter).

In the experiments of this research, it is assumed that the base stations are close to the highway ($d_{BS\ HW}$ = 20 m) and since there are no standardized LOS Blockage model for the highway scenario yet, we used the 3GPP RMa model to calculate Pr_{LOS} using Equation 17.

For generating the blockage pattern, first we calculate $Pr_{LOS}(d_{2D}(x))$. Then, assuming that the arrival rate is predefined $_B$ = 0.1 m ^{1}, we derive $_B(x)$ from the equation: $Pr_{LOS}(x) = 1 - _B \times _B(x)$. For example in Figure 4, the calculated $_B$ for the highway scenario in which a 5G base station provides cellular coverage is shown. As expected, when d_{2D} increases, the average length of the LOS blockage events increases.

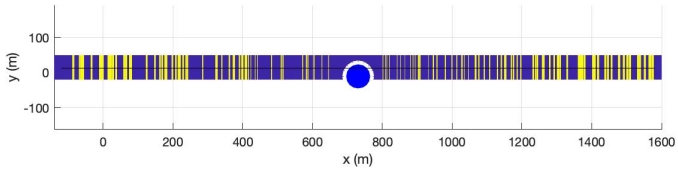

Fig. 4: A sample example of the generated blockage pattern (yellow) in a highway scenario in which a 5G base station (blue circle) provides cellular coverage.

III. Information Fusion by Kalman Filter

Kalman filter can combine different measurements and relate them with the state of a system. In a vehicle tracking problem, finding the kinematic state of the vehicle is the goal, hence we defined the state vector of the car in the form $\mathbf{x}_k = [x_k\ y_k\ \underline{x}_k\ \underline{y}_k\ \ddot{x}_k\ \ddot{y}_k]^T$ where $\underline{x}_k$ and $\underline{y}_k$ are velocity and $\ddot{x}_k$ and $\ddot{y}_k$ are acceleration. The state space model of the Kalman filter is expressed in the following equations:

$$\mathbf{x}_{k+1} = \mathbf{F}\mathbf{x}_k + \mathbf{w}_k; \tag{18}$$

$$\mathbf{z}_k = \mathbf{H}\mathbf{x}_k + \mathbf{v}_k; \tag{19}$$

where $\mathbf{F}$ is the state transition matrix of the constant acceleration process, $\mathbf{w}_k \sim \mathcal{N}(\mathbf{w}; 0; \mathbf{Q})$ is the white Gaussian process noise where $\mathbf{Q}$ is its process noise covariance matrix. $\mathbf{z}_k$ is the measurement, $\mathbf{H}_k$ is the measurement function, $\mathbf{v}_k \sim \mathcal{N}(\mathbf{v}; 0; \mathbf{R})$ is the associated measurement error [12]. The measurement update of the Kalman filter is implemented in a sequential manner. Namely, depending on the LOS blockage, state vector is updated firstly using 5G measurements and then updated using IMU measurements [13].

A. Update Using IMU Measurements

The noisy sample generation process running for IMU measurements is the same as cellular measurements generation process. Assuming $\ddot{x}_k$ and $\ddot{y}_k$ are true acceleration values of the vehicle, the samples generated in the IMU are white Gaussian noise added acceleration measurements in the form $\mathbf{z}_{IMU;k} = [a_{x;k}\ a_{y;k}]^T$ given by $a_{x;k} = _k + \ddot{x}_k$ and $a_{y;k} = !_k + \ddot{y}_k$ where $a_{x;k}$ and $a_{y;k}$ are the measured accelerations on x and y respectively and $_k \sim \mathcal{N}(0; ^2)$ and $!_k \sim \mathcal{N}(0; ^2_!)$ are white Gaussian samples. It is assumed that the measurement noise covariance $\mathbf{R}_{IMU}$ is diagonal and ideally known by the Kalman filter.

B. Update Using Cellular Network Measurements

The observations from the cellular positioning are in the form $\mathbf{z}_{CEL;k} = [r_k\ _k]^T$ consisting of range and angle data. Assuming the function $h_r(\mathbf{x}_k)$ calculates the range $\hat{r}$ from the state vector $\mathbf{x}_k$ and $h\ (\mathbf{x}_k)$ calculates the angle $\hat{}$ from the state vector, they are in the form

$$\hat{r}_k = h_r(\mathbf{x}_k) = \sqrt{(x_k - x_{BS})^2 + (y_k - y_{BS})^2}; \tag{20}$$

$$\hat{}_k = h\ (\mathbf{x}_k) = arctan\left(\frac{y_k\ \ y_{BS}}{x_k\ \ x_{BS}}\right); \tag{21}$$

where $(x_{BS}; y_{BS})$ is the position of the connected BS and the origin of the range and angle calculated based on TOA and AOD in the downlink mode. As mentioned before, due to the space mismatch, for the calculation of $\mathbf{H}_k$ the extended Kalman filter formulation should be used in the form [14]

$$\mathbf{H}_k = \frac{@\hat{\mathbf{H}}(\mathbf{x})}{@\mathbf{x}}\bigg|_{\mathbf{x}_{k|k-1}}; \tag{22}$$

where $\mathbf{x}_{kjk\ 1}$ is the predicted state and $\hat{\mathbf{H}}(\mathbf{x})$ is defined by $\hat{\mathbf{H}}(\mathbf{x}) = [h_r(\mathbf{x})\ h\ (\mathbf{x})]^T$.

In order to determine the measurement noise co-variance matrix of the cellular model $\mathbf{R}_{CEL}$, we use the calculated error bounds presented in Equations 15-16 for the noise measurement covariance in the form $\mathbf{R}_{CEL} = diag[\ ^2,\ ^2]$.

IV. Simulation Design and Environment

Due to the large number of hypothetically effective factors and scenarios, a comprehensive case study is conducted on a simple example problem. As shown in Figure 5, the example scenario consists of a vehicle moving on a highway and 5G network base stations deployed alongside the highway. On the vehicle, a 5G user terminal and an IMU is mounted and the goal is to localize the vehicle by the means of the Kalman filter.

The setup consists of an arbitrary number of base stations with the distance $d_{BS\text{-}BS}$ or inter-site distance (ISD) from each other and the distance $d_{BS\text{-}HW}$ = 20 m from the highway. Each base station's array antenna is placed in z_{BS} = 20 m height from the xy-plane and faced toward the highway with no tilt.

To challenge the proposed positioning system, a non-constant acceleration movement and trajectory are produced. As shown in Figure 5, a snake-shape trajectory with sharp turns and harsh brake intensities is created to have an extreme driving scenario, where a car with the speed of v = 130 km/h is maneuvering in curves, each with the length l_c = 20 m, and

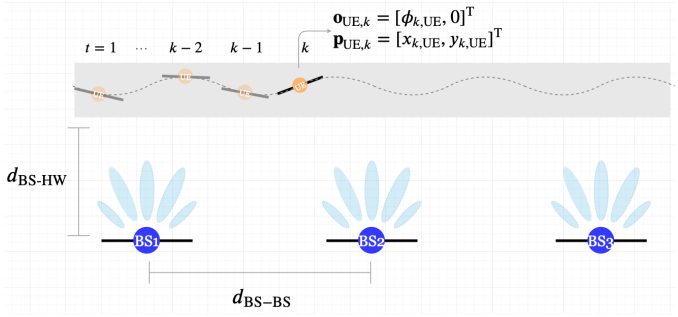

Fig. 5: Experiment setup consists of a moving car on a predefined trajectory and 3 base stations.

the width w_c = 5 m. Meanwhile, at every other turn the linear speed is reduced to i_b = 75% to simulate the car brakes.

Compared to the previous generations, 5G supports a wide range of carrier frequencies and deployment options such as the size of the base stations, massive MIMO options, and large channel bandwidths. In [15], a scalable orthogonal frequency division multiplexing (OFDM) waveform is proposed to handle a wide range of carrier frequencies and deployments. On the other hand, in 3GPP release-14 [16], one of the proposed 5G deployment scenarios is a highway scenario. In this document, it is proposed to use ISD = 500 m for 30 GHz frequency band. Combining this with the scalable OFDM waveform proposed in [15], mmWave OFDM profile is summerized in Table I, and it is considered to be analyzed in the experiments.

TABLE I: New radio (NR) mmWave settings

F_c	W_{PRB}	ISD	$P_{T,max}$	N_T
28 GHz	720 kHz	500 m	30 dBm	256

In the experiments, the number of physical resource blocks (PRB) can be less than full capacity, the transmitter power per PRB is calculated in the form: $P_{T\ per\ PRB} = P_{T,max}$=275. Then, P_T is obtained based on N_{PRB}. It should be noted that P_T does not change by N_{BS},N_{UE},N_S or N_B. Since UE is a simple and low cost device, N_{UE} is set to 4.

Other parameters are set to be similar to the 5G Tracking Reference Signal (TRS), which is used for accurate time and frequency tracking as well as path delay spread estimation in the UE [17]. TRS is sent with 4 OFDM symbols (N_S = 4) and uses 3 out of 12 available subcarriers in a PRB. Since the maximum number of PRBs (N_{PRB}) in 5G is 275, we assume the maximum N_{PRB} for TRS is 70. The cellular measurement rate r_{CEL} is also set to 80 ms.

V. Results and Analysis

A. Cellular Measurements Analysis

In this section, the accuracy of the radio measurements are studied on the highway regardless of the car and its movements. The experiment setup is shown in Figure 5, where 3 base stations are deployed 20 m far from the highway and only the accuracy of the measurements in the center cell which is affected by the interference from the both sides is studied.

Figure 6 shows the calculated error bounds for mmWave cells. When the car starts at one edge and continues to reach the other edge, the signal to interference plus noise ratio (SINR) is close to zero and increases in the center of the cell and then again decreases to zero. At the edge of the cell, where the accuracy is limited by the small SINR, phi samples has large errors. This angular inaccuracy in low SINR areas increases the maximum error of the positioning system to tens of meters and makes the positioning system unstable and non-robust.

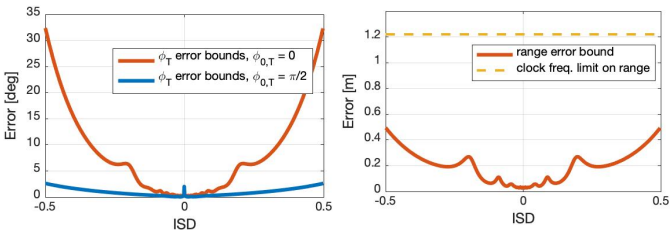

(a) Phi Error (b) Range Error

Fig. 6: Radio measurement error bounds, ISD = 500 m, N_S = 4, N_{PRB} = 70

Two factors are involved in the CRLBs of the angle: First is the SINR and it cannot be improved further and the edge of the cell; Second is the spatial information. In an array antenna based communication, the beams are less visible at the tilted angles (0 or 180) and the spatial information is small. With the experiment setup which is shown in figure 5, the edge of the cell, is where this issue happens. Therefore, we turned the BS antennas 90 as shown in Figure 7 to improve the beam resolution for these areas. Considering the fact that this does not affect the range measurements, the blue curve in Figure 6a shows the results with the new setup. The error bound at the edge of the cell is reduced to below 3 after the rotation.

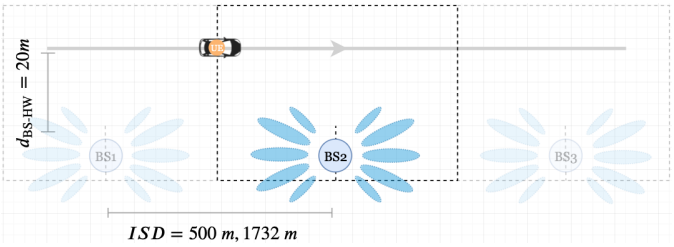

Fig. 7: New experiment setup, the BS antennas face the edge of the cell ($_{BS}$ = 90).

An important limiting factor for TOA estimation is the time resolution at the receiver. This time resolution is larger than the inverse of the radio's clock frequency and that imposes a limit on the ranging accuracy. According to the proposed NR numerology by [15], the sampling frequency at 28 GHz is F_s = 245:76 MHz. Therefore, the lower limit on the TOA error bound is 1=F_s and consequently c=F_s on the range error bound

if no oversampling or interpolation techniques are utilized. As shown in Figure 6b, dashed yellow line on 1.22 m is the receiver sampling frequency limit on the range measurements' error bound.

B. 5G/IMU Sensor Fusion System

Figure 8 shows the 5G/IMU positioning system error, when the mmWave is used. The error is calculated from the Kalman filter position estimates. In these experiments, the car passes 9 complete 5G cells shown in Figure 7. The pattern of the recorded error is periodic with 9 peaks and 9 valleys. The error peaks are due to the long distance between the BS and the UE and consequently low SINR. On the other hand, when the car becomes closer to the BS, the SINR improves and the error valleys are made.

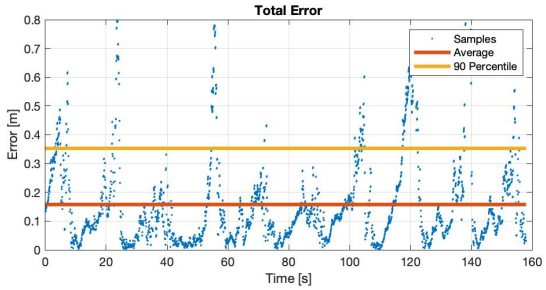

Fig. 8: mmWave/IMU sensor fusion, no sampling frequency limit, no LOS blockage, $N_s = 4$, $N_{\text{PRB}} = 70$

It can be seen that the error of each cell is different. In order to calculate one averaged error value, the same experiment is simulated 40 times and the root mean squared error (RMSE) for each time step is calculated. Then, the 90 percentile of the RMSEs are taken and reported in Figure 9.

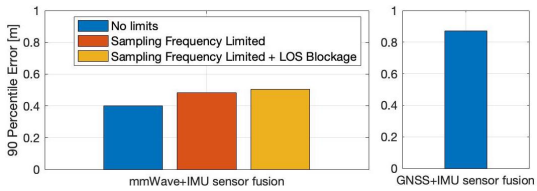

Fig. 9: 90 percentile error of different positioning algorithms after 360 Monte Carlo runs

Figure 9 shows that the 5G/IMU positioning based on the mmWave outperforms GNSS/IMU positioning due to its large available bandwidth, and large number of BS antennas. The Kalman filter and the IMU sensor fusion could keep the positioning alive during the LOS blockages where no measurements are received from the 5G side. These results show that this positioning technique is resistant to rural LOS blockages.

C. Parametric Study

The 5G cellular network model which is used in this work has various parameters influencing the performance of the positioning. In this section, 3 of them are chosen and their impact is analyzed: bandwidth or N_{PRB}, number of BS antennas N_{BS}, and number of OFDM sequential symbols N_{S}. In the following subsections the RMSE of the positioning system for 360 Monte Carlo runs is shown for different values of the parameter. In all of the experiments, these default values are set for the parameters, otherwise it is stated: $_{BS} = 90$, $N_{UE} = 4; N_s = 4$, $N_{\text{PRB}} = 70$, $_{\text{Blockage}} = 0{:}05$.

D. Bandwidth

The derived CRLBs in [7] indicate that the range error bound is inversely proportional with the bandwidth (REB $\propto 1{=}W$) which means that increasing it will decrease the range error and makes the cellular ranging more accurate. When the sampling frequency limit is applied, the ranging accuracy cannot become better than 1.22 m in mmWave. Hence, increasing the bandwidth does not affect the performance of the systems working beyond these limits. Based on the CRLBs, the maximum useful bandwidth for the mmWave when the sampling frequency is applied is 19.56 MHz or 27 PRBs.

Figure 10 shows how much accuracy gain is possible by increasing the bandwidth in each subsystem. Since the orange and yellow lines represent the positioning systems with sampling frequency limit, they remain constant when N_{PRB} exceeds 25. This observation is in line with our expectation. It can be seen from the blue lines which are not affected by the sampling frequency limit, that the major accuracy gain happens from 5 to 25 PRBs.

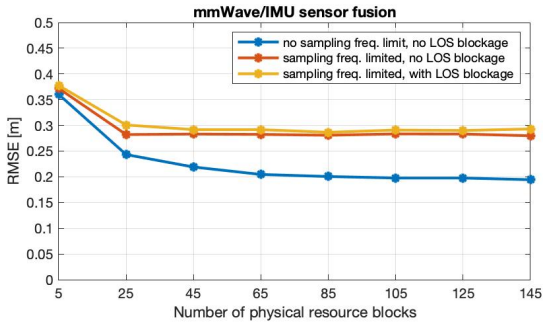

Fig. 10: mmWave/IMU positioning RMSE for different number of physical resource blocks which represents bandwidth.

E. Number of Sequential Symbols

The number of sequential OFDM symbols which is used by the signal improves the measurements but does not affect the SINR. Hence, it is an important but expensive resource. According to the CRLBs formulas in [7], both of the error bounds are inversely proportional to the root of the number of sequential symbols: REB $\propto 1{=}\sqrt{N_s}$, AEB $\propto 1{=}\sqrt{N_s}$. The default value is 4 to be similar to TRS signal. It should be noted that in the sampling frequency limited systems the range error bound does not improve despite setting large number of sequential symbols. However, since it affects both angle error bound (AEB) and range error bound (REB), the total

positioning accuracy improves. Figure 11 shows the accuracy gain by increasing N_S.

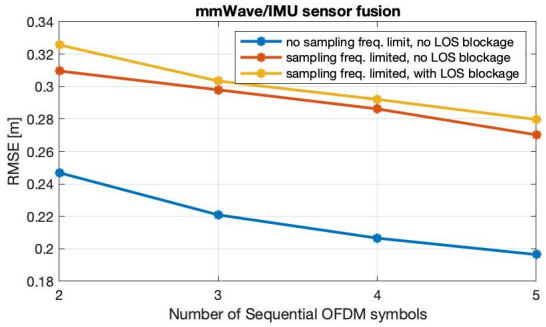

Fig. 11: mmWave/IMU positioning RMSE for different number of sequential OFDM symbols.

F. Number of BS antennas

The communication model shows that increasing or decreasing N_{BS} does not affect the SINR. If we focus on the cell edge where the SINR is zero, we reduced the error of these areas significantly by rotation of the BS antennas and increasing the spatial information. Hence, we expect to see accuracy gain due to the increase of spatial information by the N_{BS}.

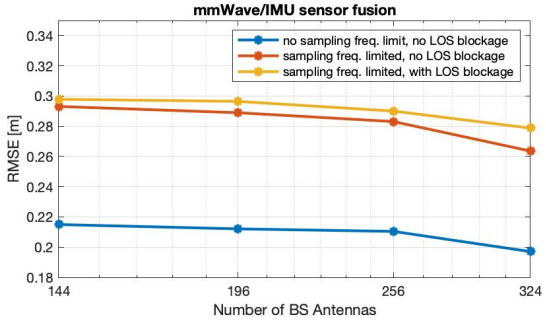

Fig. 12: mmWave/IMU positioning RMSE for different number of BS antennas.

Figure 12 demonstrates how increasing the number of the base station antennas N_{BS} affects the accuracy. It can be seen that increasing N_{BS} from 36 to 144, 4 cm accuracy gain is possible.

VI. Conclusions

In this paper, a positioning system for vehicles based on the 5G cellular network and sensor fusion is developed and analyzed. The proposed system uses URA antennas in 5G terminals, which provide range and angle measurements with respect to the base stations. The error bounds of these measurements are calculated based on the CRLB theorem. In the sensor fusion process, measurements from the cellular network are combined with IMU acceleration measurements by an extended Kalman filter.

The proposed algorithm is tested in a highway scenario by computer simulations with different propagation schemes and parameters. The results show that high accuracy single base station positioning for the 5G connected vehicles is feasible. Further simulations indicate that sub-meter wide area positioning is possible by combining mmWave with vehicle sensors.

We also showed that UE-specific algorithm implementation (e.g., sampling frequency) limits the benefit of increasing the bandwidth. Using a higher number of BS antennas, bandwidth, and the number of sequential OFDM symbols can improve the algorithm accuracy. We conclude that IMU sensor fusion is effective for compensating occasional LOS blockages.

References

[1] M. Fallgran, M. Dillinger, Z. Li, G. Vivier, T. Abbas, J. Alonso-Zarate, T. Mahmoodi, S. Alli, T. Svensson, and G. Fodor, "On selected v2x technology components and enablers from the 5gcar project," in *2018 IEEE International Symposium on Broadband Multimedia Systems and Broadcasting (BMSB)*, June 2018, pp. 1–5.

[2] K. Bengler, K. Dietmayer, B. Farber, M. Maurer, C. Stiller, and H. Winner, "Three decades of driver assistance systems: Review and future perspectives," *IEEE Intelligent Transportation Systems Magazine*, vol. 6, no. 4, pp. 6–22, winter 2014.

[3] K. Ohno, T. Tsubouchi, and S. Yuta, "Outdoor map building based on odometry and rtk-gps positioning fusion," in *IEEE International Conference on Robotics and Automation, 2004. Proceedings. ICRA '04. 2004*, vol. 1, April 2004, pp. 684–690 Vol.1.

[4] S. Kuutti, S. Fallah, K. Katsaros, M. Dianati, F. Mccullough, and A. Mouzakitis, "A Survey of the State-of-the-Art Localization Techniques and Their Potentials for Autonomous Vehicle Applications," *IEEE Internet of Things Journal*, vol. 5, no. 2, pp. 829–846, Apr. 2018.

[5] X. Cui, T. A. Gulliver, J. Li, and H. Zhang, "Vehicle Positioning Using 5g Millimeter-Wave Systems," *IEEE Access*, vol. 4, 2016.

[6] A. Kakkavas, M. H. C. Garcia, R. A. Stirling-Gallacher, and J. A. Nossek, "Performance Limits of Single-Anchor mm-Wave Positioning," *arXiv:1808.08116 [cs, math]*, Aug. 2018, arXiv: 1808.08116.

[7] Z. Abu-Shaban, X. Zhou, T. Abhayapala, G. Seco-Granados, and H. Wymeersch, "Error Bounds for Uplink and Downlink 3d Localization in 5g Millimeter Wave Systems," *IEEE Transactions on Wireless Communications*, vol. 17, no. 8, pp. 4939–4954, Aug. 2018.

[8] H. Krim and M. Viberg, "Two decades of array signal processing research: the parametric approach," *IEEE Signal Processing Magazine*, vol. 13, no. 4, pp. 67–94, July 1996.

[9] A. Shahmansoori, G. E. Garcia, G. Destino, G. Seco-Granados, and H. Wymeersch, "Position and Orientation Estimation Through Millimeter-Wave MIMO in 5g Systems," *IEEE Transactions on Wireless Communications*, vol. 17, no. 3, pp. 1822–1835, Mar. 2018.

[10] G. R. MacCartney and T. S. Rappaport, "Study on 3gpp rural macrocell path loss models for millimeter wave wireless communications," in *2017 IEEE International Conference on Communications (ICC)*, May 2017.

[11] "5g; study on channel model for frequencies from 0.5 to 100 ghz (3gpp tr 38.901 version 14.0.0)," 3rd Generation Partnership Project Technical Specification Group Radio Access Network, Tech. Rep., May 2017.

[12] Y. Bar-Shalom, X. R. Li, and T. Kirubarajan, *Estimation with applications to tracking and navigation: theory algorithms and software*. John Wiley & Sons, 2004.

[13] R. P. Mahler, *Statistical multisource-multitarget information fusion*. Artech House Norwood, MA, 2007, vol. 685.

[14] S. M. Kay, *Fundamentals of statistical signal processing*, ser. Prentice Hall signal processing series. Upper Saddle River, NJ: Prentice Hall PTR, 1993.

[15] A. A. Zaidi, R. Baldemair, H. Tullberg, H. Bjorkegren, L. Sundstrom, J. Medbo, C. Kilinc, and I. Da Silva, "Waveform and Numerology to Support 5g Services and Requirements," *IEEE Communications Magazine*, vol. 54, no. 11, pp. 90–98, Nov. 2016.

[16] "5g;study on scenarios and requirements for next generation access technologies (3gpp tr 38.913 version 14.3.0 release 14)," 3rd Generation Partnership Project Technical Specification Group Radio Access Network, Tech. Rep., 2017.

[17] S. Ahmadi, Ed., *5G NR: architecture, technology, implementation, and operation of 3gpp new radio standards*. Cambridge: Elsevier, 2019.